AN OPEN-SOURCE HYPERSONIC AERODYNAMIC AND AEROTHERMODYNAMIC MODELING TOOL

Piyush M. Mehta [(1)], Edmondo Minisci [(1)], Massimiliano Vasile [(1)], Andrew C. Walker [(2)], Melrose Brown [(3)]

[(1)] University of Strathclyde, 75 Montrose St, Glasgow G1 1XJ, UK. Email: piyush.mehta@strath.ac.uk, edmondo.minisci@strath.ac.uk, massimiliano.vasile@strath.ac.uk
[(2)] Los Alamos National Laboratory, MS D466, Los Alamos, NM 87545, USA. Email: awalker@lanl.gov
[(3)] University of New South Wales at ADFA, Canberra, Australia. Email: melrose.brown@adfa.edu.au

ABSTRACT

We present recent progress towards a Free Open Source Tool for Re-entry of Asteroids and Debris (FOSTRAD) that can perform multi-fidelity modeling of hypersonic aerodynamics and aerothermodynamics across all flow (density) regimes applicable to the re-entry of space vehicles, debris, and asteroids. FOSTRAD's capabilities are validated using Direct Simulation Monte Carlo (DSMC) and Computational Fluid Dynamics (CFD) simulations. Aerodynamic computations in the continuum and free molecular regime are performed using Modified Newtonian Theory and the free molecular analytical model of Schaaf and Chambre, respectively. Aerothermodynamic computations are performed using the semi-empirical methods of Detra-Kemp-Riddell (as used in SCARAB), Fay-Riddell, and Van Driest in the continuum regime while the free molecular analytical model is used in the free molecular regime. Computations in the transition regime are performed using the newly developed bridging formulae for aerodynamics and Legge formulae for aerothermodynamics. Results show that the proposed tool performs well in estimating both aerodynamic and aerothermodynamic properties across all flow regimes.

1. INTRODUCTION

1.1 Motivation

Earth orbiting objects (space vehicles, capsules, satellites and space debris) that re-enter the atmosphere encounter hypersonic flow during a large part of their trajectory. For space vehicles and capsules, aerodynamics and aerothermodynamics in hypersonic flow are central to the design of the vehicle, thermal protection systems (TPS), and re-entry trajectory prediction and optimization for mission planning and analysis. For satellites and space debris, aerodynamics and aerothermodynamics analysis becomes important in modeling survivability, fragmentation, re-entry trajectory, and ground impact predictions.

Accurate analysis of hypersonic aerodynamics and aerothermodynamics require high-fidelity simulations using numerical methods such as Direct Simulation Monte Carlo (DSMC) or Computational Fluid Dynamics (CFD). However, rapid computation of aerodynamic and aerothermodynamics properties is required for space vehicle trajectory optimization and satellite and space debris survivability, trajectory, or ground impact prediction. Since high-fidelity numerical methods are computationally prohibitive, a tool that uses a multi-fidelity approach to aerodynamics and aerothermodynamics modeling is required.

Well-known tools developed for satellite and debris re-entry like ORSAT [1], SCARAB [2], and DRAMA [3] are either not freely available, are not open source providing no behind-the-scene information or provide results that are very difficult to interpret. Most tools for preliminary vehicle and thermal system design are developed for the continuum regime [4,5]. Currently, no freely available tools exist for the transition flow regime. The goal of the current work is the development of FOSTRAD, an open-source, freely available multi-fidelity tool that can be used for hypersonic aerodynamics and aerothermodynamics analysis in the continuum, transition, and free molecular flow regimes. FOSTRAD can be applied to space vehicle and TPS design, trajectory optimization per mission requirements, and extended to the atmospheric entry of asteroids (but that will be a subject of future work).

1.2 Background

Aerodynamic force and moment coefficients can be characterized as the exchange of momentum between a gas flow and an object. Aerothermodynamics can be formally defined as the thermodynamic study of the interaction between a gas flow and an object. Viscous flows over a solid body result in forced convective heating at the body surface that is highly amplified for the highly hypersonic Mach numbers encountered during re-entry. Such heating poses a serious threat to vehicle integrity or offers an opportunity to dispose of defunct satellites or space debris that could pose a threat to human life on Earth upon re-entry.

Analytical and semi-empirical models for the rapid computation of aerodynamic and aerothermodynamic properties exist in both the continuum and free molecular flow regimes [2,6-10]. High-fidelity computations are also performed using numerical simulation methods. The choice of numerical method is dependent on the characterization of flow into three regimes: free molecular, transition, or continuum. The Knudsen number, Kn, defined as the ratio of the mean free path to the characteristic length scale of the object is typically used to characterize the rarefaction of the

flow. For free molecular and transition flows, DSMC, which stochastically solves the Boltzmann equation, is used while CFD, which solves the Navier-Stokes equations, is used for continuum flows. The *Kn* values at which the flow transitions from one regime to another are loosely defined. For this work, we will assume that the transition regime is defined by the *Kn* values where the aerodynamic coefficients approach the constant continuum and free molecular limits, as discussed later in this paper.

1.3 Current Work

Here, we present recent progress towards the development of FOSTRAD. This work will be directed toward space vehicles and capsules, especially validation of the tool using the Orion Crew Exploration Vehicle (CEV). We perform a comparative study to better understand the expected uncertainties.

The paper is organized in the following format: section 2 discusses the computational methods for high-fidelity simulations, section 3 discusses the aerodynamic and aerothermodynamic models and methodologies implemented in the tool, section 4 presents results, and section 5 provides conclusions.

2. COMPUTATIONAL METHODS

Hypersonic flows that occur in the harsh re-entry environment are extremely difficult to replicate in a laboratory environment. Gathering measurement data inside the shock layer on re-entry flights is restricted by the high heat and temperature of the environment. Therefore, high-fidelity data in the re-entry regime is primarily derived using computational methods such as DSMC and CFD that model the flow physics. The tool's ability to compute accurate aerodynamic and heat transfer coefficients is validated with high-fidelity simulations.

2.1 DSMC

The DSMC method, developed by Bird [11], is a computational technique for the simulation of dilute gas flows at the molecular level and is, to date, the basic numerical method in the kinetic theory of gases and rarefied gas dynamics. The DSMC method uses a cell and particle approach to track representative particles, while probabilistically selecting candidates for intermolecular collisions. The basic assumption behind the technique is that the movement and collisions of particles can be decoupled based on the dilute gas approximation. The current work uses two different DSMC solvers to observe the effect of different high-enthalpy chemistry models on surface heat transfer. Both solvers were calibrated with the same input parameters to the extent possible.

2.1.1. dsmcFoamStrath

dsmcFoamStrath is a DSMC solver within the framework of OpenFOAM, an open source C++ fluid dynamics toolbox [12]. It is a custom version developed at the University of Strathclyde [13] of the standard dsmcFoam solver included with OpenFOAM. Additional features of dsmcFoamStrath include vibrational energy modes, the quantum-kinetic (Q-K) chemical reaction model [13] for a 5-species air mixture, and a new framework for measuring macroscopic properties. With these new features, dsmcFoamStrath is state-of-the-art and suitable for application to atmospheric entry problems.

2.1.2. DAC

The DSMC Analysis Code (DAC) was developed by the National Aeronautics and Space Administration (NASA) primarily to study rarefied gas dynamic problems such as atmospheric re-entry. It is an export-controlled code only accessible to U.S. persons. DAC has the ability to automatically adapt the collision grid to resolve the local mean free path of a flow field. DAC also utilizes a pre-processor which specifies the "proper" time step and statistical weight, *W*, for representative molecules given the gas conditions such as number density and free-stream velocity. DAC employs the Total Collision Energy (TCE) model for high-enthalpy chemical reaction modeling.

2.2 CFD

CFD is a well-established collection of methods used to numerically solve the Navier-Stokes equations. Chemical and thermal non-equilibrium can be accommodated through the application of additional equations that supplement the basic mass, energy, and momentum conservation equations. The strength of CFD is the computational efficiency in which high Reynolds number flows can be simulated compared with particle-based approaches such as DSMC. Traditional CFD techniques break down as the gas becomes rarefied and non-equilibrium effects become prevalent. However, the CFD method can be usefully extended further toward the rarefied regime through methods such as the implementation of non-zero "velocity slip" boundary conditions at solid surfaces.

2.2.1 CFD++

CFD++ is a commercial 2^{nd} order accurate Total Variation Diminishing (TVD), finite volume CFD code from Metacomp Technologies [14]. The Harten Lax and van-Leer with Contact discontinuity (HLLC) scheme is used for the inviscid fluxes and Metacomp's proprietary multi-dimensional polynomial reconstruction method is applied for high-order reconstruction. Sutherland's viscosity law is applied for all simulations. The finite-rate chemical reactions are calculated using Park's 5-species, 5-reaction model [15]. Licensing restrictions preclude the use of the thermal non-equilibrium module and all simulations therefore assume the gas is in thermal equilibrium.

3. METHODOLOGY

FOSTRAD uses a panel method in which any arbitrary object geometry is modeled using small triangular facets. The number of facets used is a balance between accuracy and computation efficiency. In this particular work, the shape and curvature of the Orion capsule is captured using approximately 20,000 facets.

3.1 Aerodynamics

3.1.1 Continuum or Modified Newtonian Theory (MNT)

The contribution of each facet to aerodynamics is computed independently as a function of the local flow inclination angle, θ. The aerodynamic contribution in the continuum flow regime is computed using Modified Newtonian Theory (MNT) given as [6]:

$$C_p = C_{p_{\max}} \sin^2(\theta) \tag{1}$$

where C_p is the local pressure coefficient and $C_{p_{\max}}$ is the maximum or stagnation point pressure coefficient. The shear contribution in the continuum regime is assumed to be zero.

3.1.2 Free Molecular (FM)

The aerodynamic contribution of each facet in the free molecular (FM) regime is computed using Schaaf and Chambre's analytic model given in Eqs. 2 and 3 that accounts for both pressure and shear contributions [8].

$$C_p = \frac{1}{s^2}\left[\begin{array}{l}\left(\frac{2-\sigma_N}{\sqrt{\pi}} s\sin(\theta) + \frac{\sigma_N}{2}\sqrt{\frac{T_w}{T_\infty}}\right) e^{-(s\sin(\theta))^2} \\ + \left\{\begin{array}{l}(2-\sigma_N)\left((s\sin(\theta))^2 + \frac{1}{2}\right) \\ + \frac{\sigma_N}{2}\sqrt{\frac{\pi T_w}{T_\infty}} s\sin(\theta)\end{array}\right\}(1+erf(s\sin(\theta)))\end{array}\right] \tag{2}$$

$$C_\tau = -\frac{\sigma_T \cos(\theta)}{s\sqrt{\pi}}\left[e^{-(s\sin(\theta))^2} + \sqrt{\pi} s\sin(\theta)(1+erf(s\sin(\theta)))\right] \tag{3}$$

where C_p and C_τ are the pressure and shear coefficients, respectively, σ_N and σ_T are the normal and tangential momentum accommodation coefficients, respectively, T_w is the surface or body wall temperature, T_∞ is the free stream translational temperature, V_∞ is the object or free stream velocity, erf( ) is the error function, and s is the speed ratio given as:

$$s = \frac{V_\infty}{\sqrt{2RT_\infty}}$$

where R is the universal gas constant. The axial and normal forces are integrals of the pressure and shear stress distributions over the surface. The force and moment coefficients in the transition flow regime are computed using global bridging formulae that will be discussed in detail in Section 4.1.

3.2 Aerothermodynamics

3.2.1 Continuum

Stagnation point heat transfer in the continuum flow regime is computed using three different semi-empirical models for a comparative study [2, 9-10,16]: Detra-Kemp-Riddell (as used in SCARAB, Eq. 4), Fay-Riddell (Eq. 5), and Van Driest (Eq. 6).

Detra-Kemp-Riddell uses a Reynolds number formulation as:

$$St = \frac{2.1}{\sqrt{\mathrm{Re}_{\infty,0}}} \tag{4}$$

where St is the Stanton number, and $\mathrm{Re}_{\infty,0}$ and $\mu(T_0)$ are given by

$$\mathrm{Re}_{\infty,0} = \frac{\rho_\infty V_\infty r_N}{\mu(T_0)} \quad and \quad \frac{\mu(T_0)}{\mu(T_\infty)} = \left(\frac{T_0}{T_\infty}\right)^\omega$$

ρ_∞ and V_∞ are free stream density and velocity, respectively, r_N is the effective nose radius of the object, $\mu(T_0)$ is the stagnation point viscosity, T_0 is the stagnation point temperature, and the value of temperature exponent, ω, is 0.78.

Fay-Riddell carried out a rigorous study taking into account the dissociation effects.

$$q = 0.94(\rho_w\mu_w)^{0.1}(\rho_s\mu_s)^{0.4}(h_s - h_w)\sqrt{\left(\frac{du_e}{dx}\right)_s} \tag{5}$$

where $[\rho_w, \rho_s]$, $[\mu_w, \mu_s]$, and $[h_w, h_s]$ are density, viscosity, and enthalpy at the wall and stagnation point, respectively, and the last term is the velocity gradient at the stagnation point computed as:

$$\sqrt{\left(\frac{du_e}{dx}\right)_s} = \frac{1}{r_N}\sqrt{\frac{2(p_s - p_\infty)}{\rho_s}}$$

where (du_e/dx) is the velocity gradient, and p_s and p_∞ are stagnation point and free stream pressure, respectively.

Van Driest simplified the model of Fay-Riddell because wall properties are often difficult to calculate.

$$q = 0.94(\rho_s\mu_s)^{0.5}(h_s - h_w)\sqrt{\left(\frac{du_e}{dx}\right)_s} \tag{6}$$

The heat transfer as a function of the local inclination angle, θ, for all three models in the continuum regime is computed using Eq. 7 as used in SCARAB [2]

$$Q(\theta) = Q_{stag}(0.1 + 0.9\cos(\theta)) \quad (7)$$

3.2.2 Free Molecular

The heat transfer in the FM regime as a function of the local flow inclination angle is given as [16]:

$$q = \frac{\alpha\rho_\infty V_\infty^3}{4s^3\sqrt{\pi}} \left[\left[\left(s^2 + \frac{\gamma}{\gamma-1} - \frac{\gamma+1}{2(\gamma-1)} \frac{\exp(T_w)}{T_\infty} \right) \right] \left\{ \begin{matrix} \exp(-s^2\sin^2\theta) + \sqrt{\pi}s\sin\theta \\ [1 + erf(s\sin\theta)] \end{matrix} \right\} - \frac{1}{2}\exp(-s^2\sin^2\theta) \right] \quad (8)$$

where α is the accommodation coefficient and γ is the specific heat ratio.

4. RESULTS

4.1 Aerodynamic Validation and Bridging Formulae

The Orion geometry used for this work is derived from the geometry defined and used in [18]. The aerodynamic force and moment coefficient computations in the continuum and free molecular regimes (FMF) are validated using results for Orion computed with DACFREE presented in figures 10, 11, 15, and 16 of [18]. DACFREE is a code that computes aerodynamic forces and moments on arbitrary bodies using standard free molecular and modified Newtonian methods [19]. Figure 1 shows the data for Orion in the continuum and free molecular regimes computed with FOSTRAD. The coefficients are computed using wetted area that changes with the angle of attack and a constant characteristic length of 5.092. The moment coefficients about the centre of gravity are calculated about the point x = 1.3333, and y = 0.2414. The DSMC data at 105 km is obtained from [18]. The values computed using FOSTRAD match very accurately with those computed with DACFREE in figures 10, 11, 15, and 16 of [18].

Wilmoth *et al.*, [20] give a global bridging formula for the aerodynamic force coefficients in the transitional flow regime as a variant of Eq. 9.

$$C_{X_{trans}} = C_{X_c} + (C_{X_{fm}} - C_{X_c})\sin(\pi(a + b\log_{10}(Kn)))^2 \quad (9)$$

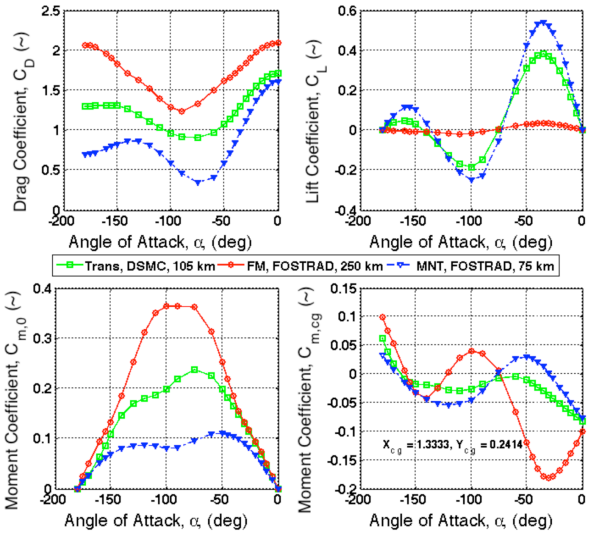

Figure 1: Continuum and Free Molecular aerodynamic values for Orion computed with FOSTRAD. DSMC data is obtained from [18].

where C_X is the force coefficient and subscripts *trans*, *fm* and *c* stand for transition, free molecular, and continuum flows, respectively. *a* and *b* are constants whose values depend on the choice of the continuum and FM limit *Kn values*.

Typically, *Kn* = 0.01 and *Kn* = 1 are used for the continuum-transition and free-molecular-transition boundaries, respectively. Fig. 2 shows the drag coefficient using the Wilmoth *et al.*, bridging function (*WM1*) for a typical range of transition *Kn* values along with DSMC data for Orion from Moss *et al.*, [18]. The DSMC data for Orion show a range on transition *Kn* values that are quite different from the typically assumed values.

The line labeled '*WM2*' in Fig. 2 shows the Wilmoth *et al.*, bridging function for a *Kn* range of 0.0001 to 100. *WM2* does a better job at tracking the Orion data for high *Kn* values but fails to track the data closely at low *Kn* values. *WM2* fails for low *Kn* values where the aerodynamic forces can cause large perturbations because of the non-flexible nature of the basis function used.

In order to track the data more closely, new bridging formulae based on the sigmoid (base 10) function are developed given as:

$$C_{X_{trans}} = C_{X_c} + (C_{X_{fm}} - C_{X_c}) \left(\begin{matrix} a_{s1}sig_{10}(b_{s1}\log_{10}(Kn) + c_{s1}) \\ + a_{s2}sig_{10}(b_{s2}\log_{10}(Kn) + c_{s2}) \\ + a_{s3}sig_{10}(b_{s3}\log_{10}(Kn) + c_{s3}) + \delta \end{matrix} \right) \quad (10)$$

where $(a\text{-}c)_{s(1,2,3)}$ and δ are fitting constants and

$$sig_{10}(x) = \frac{1}{1 + 10^{(-/+)x}}$$

The sign in the exponent depends on the trend of the variation of the aerodynamic coefficient with *Kn*, with the sign being negative for an increasing trend. The choice of the number of sigmoid functions in the function used is based on the desired level of accuracy. Depending on the number of sigmoid functions used, the unused constants in Eq. 10 can be set to zero. For example, if only a single sigmoid basis functions is able to track the data with the desired accuracy, then $(a\text{-}c)_{s(2,3)}$ will be set to zero.

The new bridging functions will henceforth be called New Sigmoid 1 (*NS1*), New Sigmoid 2 (*NS2*), and New Sigmoid 3 (*NS3*) depending on the number of sigmoid functions used. The sigmoid function is chosen because it is more flexible as shown in Fig. 2. The bridging functions developed using the Orion data are plotted in Fig. 2. Table 3 and 4 give the lift, drag and moment coefficients for Orion from Moss and those calculated in FOSTRAD using the different bridging functions. Fig. 3 shows the percentage errors in Orion C_D using the Wilmoth *et al.* and newly derived sigmoid bridging functions compared to high fidelity numerical methods.

As expected, the new *NS2* and *NS3* functions lower the maximum error from ~10% (with the Wilmoth et al. bridging functions) to ~2%, and performs significantly better at low *Kn* values where aerodynamic forces become increasingly relevant.

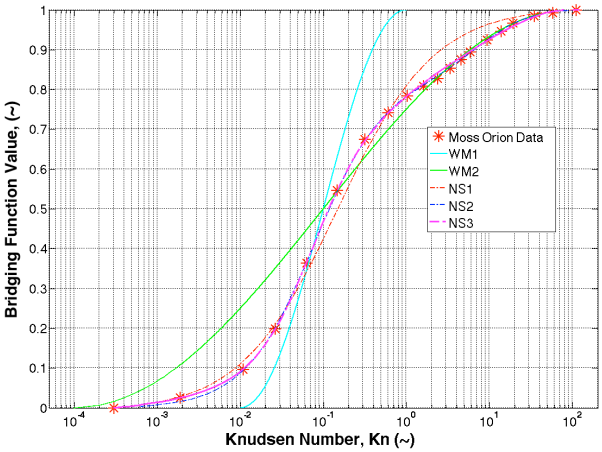

Figure 2: Wilmoth et al. [20] *and the newly derived sigmoid bridging functions plotted with data for Orion* [18].

The ~2% errors are because FOSTRAD C_D at each *Kn* is computed using a non-constant C_{Dc} and C_{Dfm} as a result of changing simulation parameters (atmospheric and wall properties), whereas, the bridging functions are derived by fitting to constant values of C_{Dc} and C_{Dfm}.

Table 1: Lift and Drag Coefficients for Orion computed with FORSTRAD using different bridging formulas. Also given are Moss DSMC values [18,20].

Kn	***Drag Coefficient, C_D***							***Lift Coefficient, C_L***					
	Moss	***WM1***	***WM2***	***NS1***	***NS2***	***NS3***	***NS2 Const***	***Moss***	***WM2***	***NS1***	***NS2***	***NS3***	***NS2 Const***
3.00E-04	1.200	1.225	1.225	1.225	1.225	1.225	1.200	0.461	0.489	0.489	0.489	0.489	0.461
1.90E-03	1.217	1.225	1.306	1.246	1.237	1.244	1.211	0.448	0.444	0.477	0.476	0.477	0.448
1.08E-02	1.266	1.225	1.412	1.376	1.292	1.295	1.264	0.412	0.377	0.443	0.443	0.439	0.416
2.63E-02	1.336	1.299	1.477	1.469	1.368	1.365	1.338	0.386	0.336	0.410	0.411	0.412	0.385
6.29E-02	1.449	1.469	1.543	1.578	1.485	1.484	1.451	0.347	0.292	0.364	0.366	0.370	0.343
1.47E-01	1.575	1.671	1.609	1.678	1.609	1.611	1.573	0.288	0.249	0.306	0.309	0.310	0.288
3.18E-01	1.663	1.829	1.668	1.748	1.698	1.697	1.661	0.229	0.210	0.249	0.247	0.247	0.228
6.01E-01	1.709	1.908	1.714	1.796	1.746	1.744	1.710	0.184	0.179	0.203	0.199	0.200	0.184
1.02E+00	1.738	1.924	1.748	1.825	1.770	1.770	1.738	0.152	0.153	0.167	0.165	0.165	0.152
1.61E+00	1.755	1.920	1.775	1.845	1.786	1.790	1.757	0.126	0.133	0.139	0.138	0.138	0.128
2.38E+00	1.768	1.917	1.796	1.858	1.799	1.805	1.772	0.110	0.116	0.119	0.118	0.119	0.110
3.35E+00	1.785	1.914	1.814	1.867	1.811	1.817	1.786	0.096	0.102	0.103	0.103	0.103	0.096
4.52E+00	1.800	1.912	1.828	1.874	1.823	1.828	1.800	0.086	0.091	0.091	0.092	0.091	0.086
5.90E+00	1.813	1.910	1.840	1.879	1.835	1.837	1.812	0.078	0.082	0.082	0.082	0.082	0.078
9.36E+00	1.834	1.908	1.858	1.882	1.855	1.853	1.834	0.066	0.068	0.068	0.069	0.068	0.066
1.38E+01	1.849	1.906	1.871	1.887	1.870	1.866	1.851	0.058	0.058	0.059	0.059	0.059	0.058
1.94E+01	1.863	1.904	1.880	1.891	1.880	1.876	1.862	0.051	0.050	0.053	0.053	0.052	0.052
3.48E+01	1.875	1.902	1.892	1.895	1.892	1.890	1.876	0.044	0.040	0.043	0.043	0.043	0.044
5.74E+01	1.881	1.900	1.897	1.897	1.896	1.898	1.882	0.039	0.035	0.038	0.037	0.037	0.039
1.11E+02	1.886	1.898	1.898	1.898	1.898	1.898	1.886	0.035	0.032	0.032	0.032	0.032	0.035

The errors using *NS2* and constant values of C_{Dc} = 1.2 and C_{Dfm} = 1.886 (*NS2 constant*) are also plotted in Fig. 3 and show that the errors are on the order of ~0.5%.

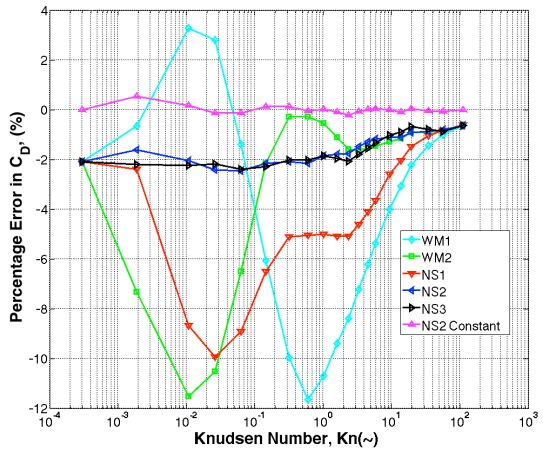

Figure 3: *Percentage error in the transition regime Orion drag coefficients using Wilmoth et al.,* [20] *and New Sigmoid 1, 2, and 3 functions.*

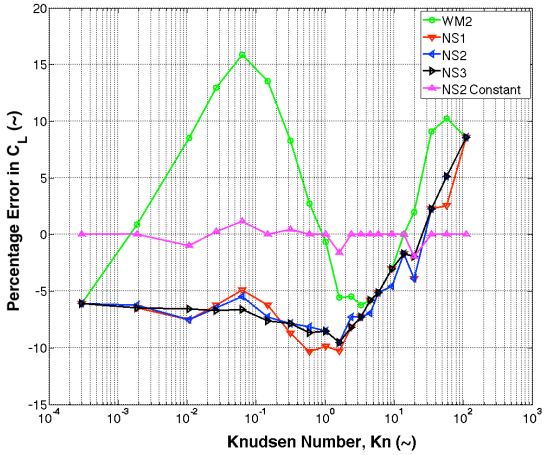

Figure 4: *Percentage error in transition regime Orion lift coefficients using Wilmoth et al.* [20]*, and New Sigmoid 1, 2, and 3 functions.*

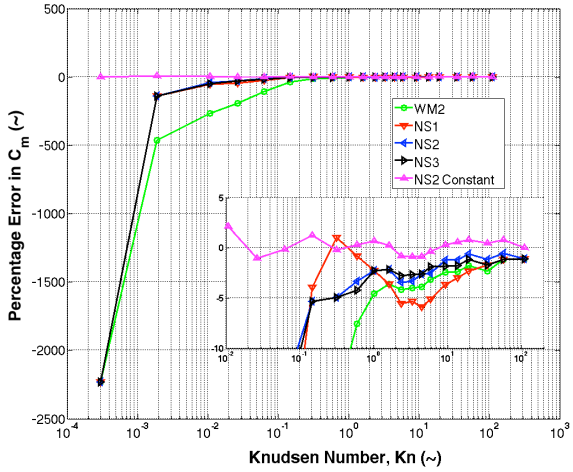

Figure 5: Percentage error in transition regime Orion moment coefficients using Wilmoth et al., [20] *and New Sigmoid 1, 2, and 3 functions*

Fig. 4 shows the percentage errors in Orion C_L using the Wilmoth et al. and newly derived sigmoid bridging functions compared to high fidelity numerical methods. As expected, the new *NS2* and *NS3* functions lowers the maximum error from ~16% (with the *WM2* bridging function) to ~9% and in general performs better at low *Kn* values.

Table 2: Moment Coefficients for Orion computed with FORSTRAD using different bridging formulas. Also given are Moss DSMC values [18].

Moss	***WM2***	***NS1***	***NS2***	***NS3***	***NS2 Const***
-0.177	-0.179	-0.179	-0.179	-0.179	-0.177
-0.176	-0.178	-0.178	-0.177	-0.178	-0.175
-0.173	-0.177	-0.176	-0.175	-0.176	-0.172
-0.170	-0.173	-0.174	-0.171	-0.172	-0.169
-0.167	-0.171	-0.172	-0.169	-0.170	-0.166
-0.163	-0.167	-0.169	-0.165	-0.166	-0.163
-0.157	-0.162	-0.165	-0.161	-0.160	-0.158
-0.153	-0.159	-0.162	-0.157	-0.157	-0.154
-0.149	-0.155	-0.157	-0.154	-0.153	-0.150
-0.144	-0.150	-0.152	-0.149	-0.148	-0.145
-0.139	-0.144	-0.144	-0.142	-0.142	-0.139
-0.131	-0.137	-0.134	-0.134	-0.134	-0.130
-0.119	-0.128	-0.120	-0.123	-0.124	-0.119
-0.101	-0.116	-0.100	-0.106	-0.106	-0.101
-0.073	-0.101	-0.076	-0.077	-0.077	-0.072
-0.041	-0.085	-0.052	-0.047	-0.048	-0.041
-0.023	-0.068	-0.034	-0.030	-0.030	-0.024
-0.014	-0.052	-0.022	-0.020	-0.021	-0.014
-0.0046	-0.026	-0.011	-0.011	-0.011	-0.0042
-0.0003	-0.007	-0.007	-0.007	-0.007	-0.0003

Fig. 5 shows the percentage errors in Orion $C_{m,c.g.}$ using the Wilmoth et al. and newly derived sigmoid bridging functions compared to high fidelity numerical methods. Again, as expected the newly developed bridging functions improve the overall performance. The large errors towards the continuum *Kn* values are due to the lack of shear in the MNT formulation combined with the order of magnitude of the values themselves, which are 3 to 4 orders of magnitude lower than C_D and C_L.

4.2 Aerothermodynamic Validation and Bridging Formulae

The different aerothermodynamic empirical models are validated with the stagnation point heat transfer coefficients from CFD in the continuum regime and DSMC in the transition regime. The bridging formulae by Legge [20] is used in the transition regime given as:

$$Q_{stag(trans)} = \frac{Q_{stag(cont)}}{\sqrt{1+\left(\frac{Q_{stag(cont)}}{Q_{stag(fm)}}\right)^2}} \quad (11)$$

Fig. 6 compares Orion stagnation point heat transfer coefficients, C_h, computed using different computational and empirical methods. Simulations for the aerothermodynamic comparison study are performed using the parameters given in Table 3.

Table 3: Simulation parameter values for CFD and DSMC

Property	Value
Free-Stream Velocity, V_∞	7.5 km/s
Atmospheric Composition	80% N_2, 20% O_2
Surface Temperature, T_w	1000 K
Free-Stream Temperature, T_∞	300 K
Number Densities	5E+21, 1E+21, 5E+20, 5E+19, 2.6E+19, 1E+19, 5E+18, 1E+18, and 5E+17
Corresponding Altitudes (US Standard Atmosphere)	62, 73, 78, 88, 92, 95, 100, 105, 115, and 120 km

All of the CFD and DSMC simulations are performed using a chemically reacting gas while the analytical models consider dissociation of the gas but not recombination. DSMC simulations are performed for a non-catalytic wall condition, whereas, CFD simulations are performed for both non-catalytic and catalytic wall boundary conditions.

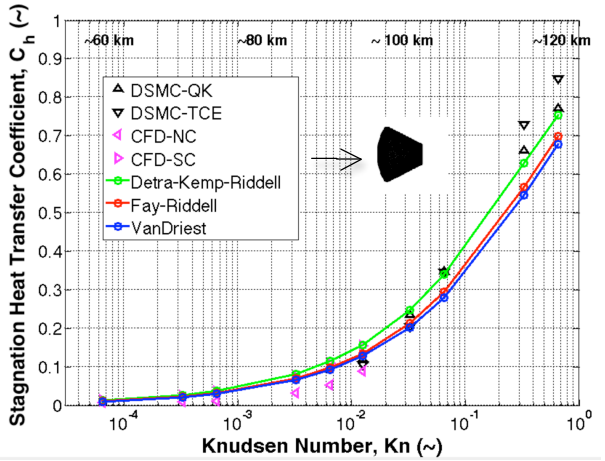

Figure 6: Orion Stagnation point heat transfer coefficients computed using different computational and empirical methods.

It can be seen that in the continuum regime, the non-catalytic and catalytic values of the stagnation point heat transfer bound the analytical model values with the variation increasing with Kn. There is no such trend in the transition regime; however, just like in the continuum regime the variation increases with Kn. The real value of the stagnation point heat transfer is expected to lie somewhere between the catalytic and non-catalytic solution which seems to be well represented by Fay-Riddell and Van Driest models. However, in the transition region, tools to perform catalytic wall simulations are not available and hence an upper bound is unknown. Also, non-catalytic wall simulations that should represent a lower bound provide values that are higher than all analytical models; especially at high *Kn*. Therefore, catalytic wall DSMC simulation and improving bridging functions for aerothermodynamics will be subject of future work.

5. Conclusions

Recent progress towards the development of a Free Open Source Tool for Re-entry of Asteroids and Debris (FOSTRAD) has been presented. Comparison of the analytical and numerical methods for calculating aerodynamic and aerothermodynamic properties across all flow regimes (free-molecular, transition and continuum) has been performed. The accuracy and variance of the analytical methods has been examined for uncertainty quantification.

FOSTRAD computes aerodynamic and properties for free molecular and continuum flows using free-molecular and modified Newtonian theory models, respectively. Global bridging formula is used for the transition regime. FOSTRAD aerodynamic computations in the free molecular and continuum regime are validated for Orion using comparison with DACFREE. New bridging formulae are developed for aerodynamics in the transition regime based on sigmoid functions. The newly developed formulae reduce the maximum error in drag coefficient for Orion down to ~2% from ~10% when compared with the previously used bridging formulae of Wilmoth et al. and perform significantly better at lower Knudsen number where the aerodynamic forces become increasingly relevant. Maximum error in lift coefficient is reduced down to ~9% from ~16% level.

FOSTRAD computes aerothermodynamic properties in the free molecular flow regime using the free-molecular analytical model while three different models of Detra-Kemp-Riddell (as used in SCARAB), Fay-Riddell and Van Driest are used in the continuum regime. Bridging formulae by Legge is used in the transition regime. Stagnation point heat transfer values computed with CFD and DSMC in the continuum and transition regime are used for comparison. CFD simulations are performed for both non-catalytic and super-catalytic wall boundary conditions with chemically reacting gas. DSMC simulations are performed using two different gas chemistry models for non-catalytic wall boundary conditions.

The non-catalytic and super-catalytic wall boundary

condition values form upper and lower bounds, respectively, around the Fay-Riddell and Van Driest analytical models, while Detra-Kemp-Riddell values are larger than the super-catalytic values. The analytical models compare well with CFD at low Knudsen number but the variance increases with increasing Knudsen number. The transition region has higher differences between DSMC and analytical models than continuum with the variance still increasing with Knudsen number.

6. Acknowledgements

Funding for Piyush Mehta is provided by the European Commission through the Marie Curie Initial Training Network (ITN) FP7-PEOPLE-2012-ITN. The authors would like to acknowledge the use of the High Performance Computing Resources 'ARCHIE' at the University of Strathclyde and the National Computing Infrastructure Facility in Australia. We would like to thank Richard Martin for help with using the HPC. The authors would also like to thank Tom Scanlon for sharing dsmcFoamStrath.

7. References

1. Rochelle, W.C., Kirk, B.S., Ting, B.C., *User's Guide for Object Reentry Analysis Tool (ORSAT) Version 5.0*, vol. 1, JSC- 28742, NASA Lyndon B. Johnson Space Center, 1999.
2. Koppenwallner, G., Fritsche, B., Lips, T., and Klinkrad, H., SCARAB – A multi-disciplinary code for destruction analysis of space-craft during re-entry, Proceedings of the 5th European Symposium on Aerothermodynamics for Space Vehicles, 8-11 Nov, 2005, Cologne, Germany.
3. Martin, C., et al., A Debris Risk Assessment Tool Supporting Mitigation Guidelines, Proceedings of the 4th European Conference on Space Debris (ESA SP-587), ESA/ESOC, Darmstadt, Germany, 18-20 April, 2005.
4. Gentry, A.E., Smyth, D.N., Oliver, W.R., The Mark IV Supersonic-Hypersonic Arbitrary-Body Program. Volume I. User's Manual, Douglas Aircraft Corporation, Long Beach, CA., 269 pp., 1973.
5. Kinney, D.J., "Aerothermal Anchoring of CBAERO Using High Fidelity CFD", 45th AIAA Aerospace Sciences Meeting, Reno, NV, January, 2007.
6. Newton, I., Principia – Mote's Translation Revised, University of California Press, 1946.
7. Anderson, J.D., Hypersonic and High Temperature Gas Dynamics, AIAA, 1989.
8. Schaaf, S.A., and Chambre, P.L., Flow of Rarefied Gases, High Speed Aerodynamics and Jet Propulsion, Princeton Univ. Press, Princeton, NJ, 1958, pp. 1–55.
9. Fay, J. A., and Riddell, F. R., "Theory of Stagnation Point Heat Transfer in Dissociated Air," *Journal of the Aeronautical Sciences*, Vol. 25, No. 2, 1958, pp. 73–85.
10. Van Driest, E.R., The problem of aerodynamic heating, Aero. Eng. Rev., Vol. 15, No. 10, Oct 1956, pp. 26-41.
11. Bird, G.A. Chemical Reactions in DSMC. AIP Conference Proceedings, 1333, 1195, 2011.
12. www.openfoam.org
13. Scanlon, T. J., Roohi, E., White, C., Darbandi, M., Reese, J. M. An open source, parallel DSMC code for rarefied gas flows in arbitrary geometries. Computers and Fluids, 39(10), 2078-2089, 2010.
14. Goldberg, U., Batten, P., Palaniswamy, S., Chakravarthy, S., and Peroomian, O., "Hypersonic Flow Predictions Using Linear and Nonlinear Turbulence Closures," Journal of Aircraft, Vol. 37, 2000, pp. 671–675.
15. Park, C., "On Convergence of Computation of Chemically Reacting Flows," AIAA Paper 85-0247, 23rd Aerospace Sciences Meeting, January 14-17, 1985.
16. Detra, R. W., Kemp, N. H., and Riddell, F. R., Addendum to Heat Transfer to Satellite Vehicles Reentering the Atmosphere, Jet Propulsion, Vol. 27, No. 12, 1957, pp. 1256-1257.
17. Regan, F. J., and AnandaKrishnan, S. M., Dynamics of Atmospheric Re-Entry, AIAA Education Series, 1993.
18. Moss, J. N., Boyles, K. A., and Greene, F. A., Orion Aerodynamics for Hypersonic Free Molecular to Continuum Conditions, 14th AIAA/AHI International Space Planes and Hypersonic Systems and Technologies Conference, 6-9 November, 2006, Canberra, Australia.
19. Wilmoth, R. G., DACFREE: A Free-Molecular/Newtonian Code for Hypersonic Flow, A Users Guide," 1999.
20. Wilmoth, R. G., Mitcheltree, R. A., and Moss, J. N., Low Density Aerothermo dynamics of the Stardust Sample Return Capsule, Journal of Spacecraft and Rockets, Vol. 36, No. 3, 1999, pp. 436-441.
21. Legge, H., Hypersonic approximations for heat transfer and shear stress applied to continuum and rarefied plume impingement, DFVLR-IB 222-87 A23, 1987.